The final publication is available at Springer via http://dx.doi.org/10.1007/s11340-016-0211-9

Fracture Characterization of Rolled Sheet Alloys in Shear Loading: Studies of Specimen Geometry, Anisotropy, and Rate Sensitivity

A. Abedini*, C. Butcher, M.J. Worswick

Department of Mechanical and Mechatronics Engineering, University of Waterloo, Waterloo, ON, CANADA

*Corresponding author: Email: aabedini@uwaterloo.ca Tel: +19056266703 Fax: +15198886197

Abstract: Two different shear sample geometries were employed to investigate the failure behaviour of two automotive alloy rolled sheets; a highly anisotropic magnesium alloy (ZEK100) and a relatively isotropic dual phase steel (DP780) at room temperature. The performance of the butterfly type specimen (Mohr and Henn, 2007; Dunand and Mohr, 2011) was evaluated at quasi-static conditions along with that of the shear geometry of Peirs *et al.* (2012) using *in situ* digital image correlation (DIC) strain measurement techniques. It was shown that both test geometries resulted in similar strain-paths; however, the fracture strains obtained using the butterfly specimen were lower for both alloys. It is demonstrated that ZEK100 exhibits strong anisotropy in terms of failure strain. In addition, the strain rate sensitivity of fracture for ZEK100 was studied in shear tests with strain rates from quasi-static (0.01 s^{-1}) to elevated strain rates of 10 s^{-1} and 100 s^{-1}, for which a reduction in fracture strain was observed with increasing strain rate.

Keywords: Fracture Characterization; Sheet Metal, Simple Shear; Rate Sensitivity

1. Introduction

The automotive industry is experiencing ever-increasing demand to reduce vehicle weight to address issues of energy conservation and environmental protection. Vehicle lightweighting can be accomplished using a variety of methods, with the main approaches involving a shift towards advanced high strength steels (AHSS) to produce thinner components or through the adoption of low density alloys such as aluminum and magnesium. Advanced high strength steels can have complex microstructures that generally trade ductility for higher strength while automotive

aluminum and magnesium alloys exhibit similar strength-to-weight ratios to steels but are anisotropic with relatively low room temperature formability and ductility. As a result, these alloys require extensive material characterization to develop and calibrate advanced constitutive models and fracture criteria for use in design of metal forming processes and crashworthiness simulation for automotive applications.

The development of stress state-dependent fracture surfaces and damage models to predict failure in automotive forming and crash simulations has created great interest and has led to the development of experimental tests to characterize failure under constant stress states [1-3]. The shear loading condition is critical to the development of the fracture surface since it corresponds to the origin of the fracture surface with a stress triaxiality and Lode parameter of zero. The shear fracture mechanism is also different from that in uniaxial tension since deformation is not limited by the onset of necking that triggers void nucleation and coalescence in many ductile materials. Shear and tensile loading conditions are complementary and opposite in nature as the stress tensor in uniaxial tension only contains symmetric stress components while shear loading only involves anti-symmetric (deviatoric) components.

Often, the shear response of ductile materials is determined by conducting torsion tests on thin walled tubular samples [4-7] or using a compact forced-simple-shear specimen for bulk materials [8]; however, such tests are not suitable for sheet materials. Iosipescu [9] designed one of the first methods for the shear testing of sheet materials by using notched specimens subjected to four-point bending. More recent studies utilized a rectangular specimen that is mechanically clamped on opposite sides with a shear deformation applied by moving the clamps parallel to each other in opposite directions. This test requires a special device that consists of two rigid parts with one piece remaining fixed and the other moving vertically or horizontally. This method of shear testing and its extensions have been used to study the shear response of a large number of sheet metals [10-15]. The so-called butterfly specimen [16-17] is a modification of these types of specimen.

Alternatively, a number of experimental studies have involved designing complex test geometries with the aid of finite element simulations where a tensile load is converted to a shear stress in the gauge area of the samples [18-28]. The principal advantage of these geometries is that the shear tests can be readily performed using conventional tensile test frames. Recently, a

novel shear sample geometry of this type was introduced by Peirs *et al*. [27] for both quasi-static and dynamic loading conditions. The design of this geometry is an evolution of the geometries proposed by Bao and Wierzbicki [18] and Tarigopula *et al*. [19]. The advantage of this test geometry is that it has a relatively simple design and does not require through-thickness machining that may introduce surface defects. Recent works by Abedini *et al*. [29] and Rahmaan *et al*. [30] have demonstrated the advantages of the Peirs *et al*. [27] geometry.

Shear characterization of materials at elevated rates of strain is also critical for accurate modelling of sheet metal forming and vehicle crash simulations. Shear testing under dynamic strain rates were initially performed by Campbell and Fergusen [31] by means of a double-notched specimen. The double-notched specimens were further used and modified in the literature to obtain a more homogeneous shear strain in the gauge area of the specimen [32-38]. Although the double-notched specimens can be utilized for shear characterization of isotropic materials, it may complicate the interpretation of the response of anisotropic materials because the shear bands in each gauge section rotate in opposite directions, complicating the interpretation of the response and potentially averaging away some of the material anisotropy. Similar statements can be made for the so-called "smiley" specimens [3, 39] in which the rotation of the shear bands have similar characteristics to that of the double-notched specimen. Furthermore, machining defects and small misalignments in the test frame can cause deformation to localize and initiate in one of the two gauge regions so that deformation is not uniform in both regions.

The objective of the present work is to investigate the influence of the shear test geometry on the fracture behaviour of automotive sheet materials. To this end, two automotive alloys of the same gauge were selected with very different properties: a highly anisotropic rare-earth magnesium alloy, ZEK100, and a relatively isotropic dual phase steel, DP780. The DP780 steel was selected since it is commonly used in automotive applications and to provide contrast with ZEK100 that possesses unique mechanical properties such as evolving anisotropy. The present work will compare the shear geometry of Peirs *et al*. [27] with the butterfly shear test geometry of Duand and Mohr [17] under quasi-static conditions. In addition, the fracture response of ZEK100 is investigated under elevated strain rates. The consideration of these two materials (ZEK100 and DP780) with properties at either end of the automotive lightweighting spectrum

will better enable the selection of appropriate test geometry for shear characterization of sheet alloys.

2. Materials

Two types of rolled sheet alloys with a nominal thickness of 1.55 mm were used in the present study, a rare-earth magnesium alloy ZEK100 (O-temper) and a commercial dual phase steel, DP780. The chemical compositions for ZEK100 and DP780 are presented in Table 1 and Table 2, respectively. Winkler *et al*. [40] have reported that the same lot of DP780 material contains 7% martensite and 30% bainite, with the remainder being ferrite. The ZEK100 alloy is known to exhibit anisotropic response in uniaxial tension and compression loading conditions as well as strong tension-compression asymmetry [41]. In order to avoid any natural ageing of the materials, all the tests reported in this paper were performed within the same week.

Table.1. Chemical composition of ZEK100.

Chemical composition (%wt)	**Zn**	**Nd**	**Zr**	**Mn**	**Mg**
	1.3	0.2	0.25	0.01	balance

Table.2. Chemical composition of DP780.

Chemical composition (%wt)	**Mn**	**Cr**	**Si**	**Mo**	**C**	**Fe**
	1.99	0.26	0.26	0.15	0.14	balance

3. Experiments and Methodology

3.1. Quasi-static Condition

Peirs *et al*. [27] developed the novel shear geometry shown in Figure 1 from a systematic finite element study to design a simple shear test specimen. Due to the small size of the sample,

throughout this paper, it will be referred to as the "mini-shear specimen". The specimen geometry was designed so that the applied tensile load is converted to a shear stress in the gauge section of the specimen. The notches are offset by an eccentricity of 1 mm to provide a stress triaxiality very close to the theoretical value of zero for shear loading [27]. This geometry has several advantages over its counterparts in the literature. Its small geometry makes it suitable for testing at higher strain rates. Furthermore, it has a rather simple geometry that is easy to fabricate. Contrary to a number of shear sample geometries in the literature [17, 18, 20, 21, 26], it does not have a reduced thickness in the shear zone which avoids complications such as machining-induced surface defects and residual stresses that can initiate fracture.

The mini-shear samples were fabricated by CNC machining using a 0.8 mm diameter flat end mill. For DP780, the specimens were manufactured with the applied load in the transverse direction (90° with respect to the rolling direction). The shear experiments for DP780 were only conducted in one direction due to the relative isotropy of the material [29]. For the anisotropic ZEK100, shear samples were fabricated to have the applied load in the 45°, 90°, and 135° directions with respect to the rolling direction. Note that as shown by Lopes *et al*. [42] for shear tests on rolled sheet, the principal stresses have the same magnitudes and directions in the 0° and 90° orientations with respect to the rolling directions. Consequently, shear tests in the 0° and 90° orientations are equivalent; therefore, only tests in the 90° orientation, along with the 45° and 135° orientations, were performed in the present study.

The von Mises equivalent strain rate, $\dot{\varepsilon}_{eq}$, was used to define the strain rate for both the DP780 and ZEK100 and is defined as:

$$\dot{\varepsilon}_{eq} = \frac{2}{\sqrt{3}}\sqrt{\dot{\varepsilon}_1^{\,2} + \dot{\varepsilon}_2^{\,2} + \dot{\varepsilon}_1\dot{\varepsilon}_2} \tag{1}$$

where $\dot{\varepsilon}_1$ and $\dot{\varepsilon}_2$ are the principal strain rate components. The von Mises equivalent strain, ε_{eq}, was calculated by integrating the equivalent strain rate using the measured DIC time increments.

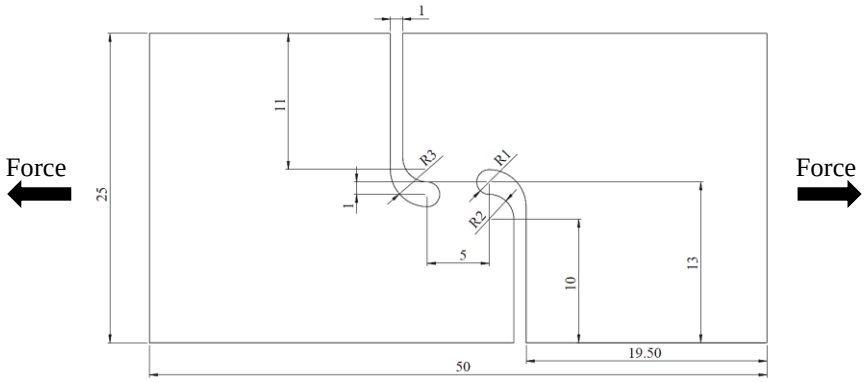

Fig.1. Mini-shear specimen geometry of Peirs *et al*. [27]. All dimensions are in millimeters.

The quasi-static tests for the mini-shear specimen were performed with an Instron model 1331 servo-hydraulic testing machine with a cross-head velocity of 0.03 mm/s to obtain a von Mises equivalent true strain rate of 0.01 s^{-1}. Note that the mini-shear specimen can be used to obtain the constitutive elastoplastic behaviour of materials under shear loading [27, 29]; however, the present paper is focused on obtaining the fracture response of the materials using the mini-shear as well as butterfly specimens.

Figure 2 shows a schematic of the so-called butterfly test specimen adopted from Mohr and Henn [16] and Dunand and Mohr [17]. The specimen features a sharp reduction in thickness between the gauge section and the specimen shoulder. This versatile specimen was specifically designed to characterize fracture over a range of plane stress states under quasi-static loading conditions. The boundaries of the specimen are curved to avoid crack initiation at the gauge section boundaries.

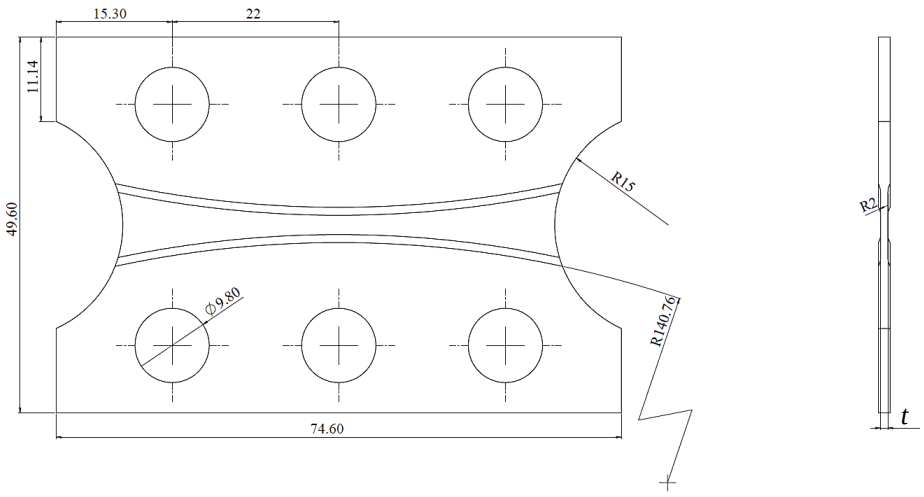

Fig.2. Butterfly specimen geometry (adopted from Dunand and Mohr [17]). All dimensions are in millimeters.

The experiments were performed using a custom-made testing device, shown in Figure 3, that consists of a moveable and a fixed portion labeled as '1' and '2', respectively. The moveable portion slides vertically along a guidance rod; whereas the fixed portion is rigidly connected to the frame of the testing machine. The butterfly specimen is clamped by tightening bolts on the knurled gripping blocks to prevent slippage during the test. Using this system, the loading condition can be controlled by the orientation of the specimen with respect to the vertical axis of the apparatus. The significant advantage of the butterfly test is that stress states from shear to plane strain conditions can be obtained using only a single test geometry [16]. Only the shear loading condition is considered in the present study to provide an alternate geometry to the mini-shear specimen.

It is important to note that contrary to the testing fixture of Dunand and Mohr [17] that employed a dual actuator system, the fixture shown in Figure 3 is a displacement-controlled apparatus. However, in shear loading, the difference between the load- and displacement-controlled systems is expected to be small as it is not a mixed deformation mode that requires balancing of the transverse stress using a second actuator. To provide context into the performance of the displacement-controlled apparatus relative to the load-controlled, in Figure 4 we have reported the horizontal forces as well as the vertical loads for a DP780 butterfly test in

the displacement-controlled apparatus. It can be seen that the vertical force is small compared to the horizontal force as expected for a shear loading condition to a load ratio of ~0.007.

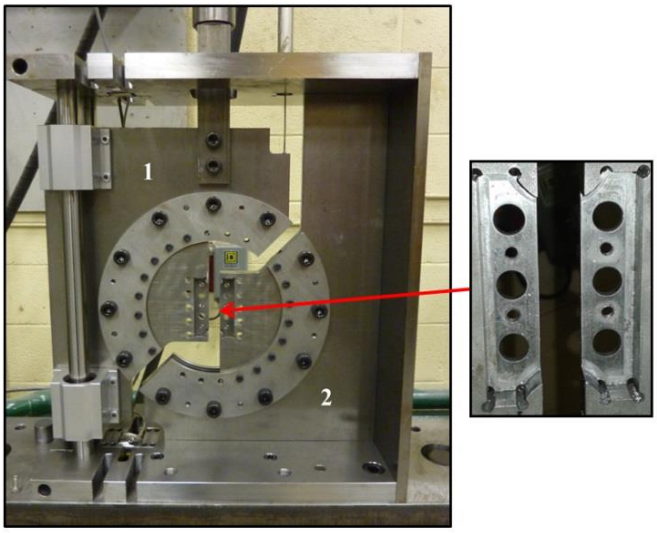

Fig.3. Testing device for the butterfly specimen (adopted from Mohr and Henn [16]).

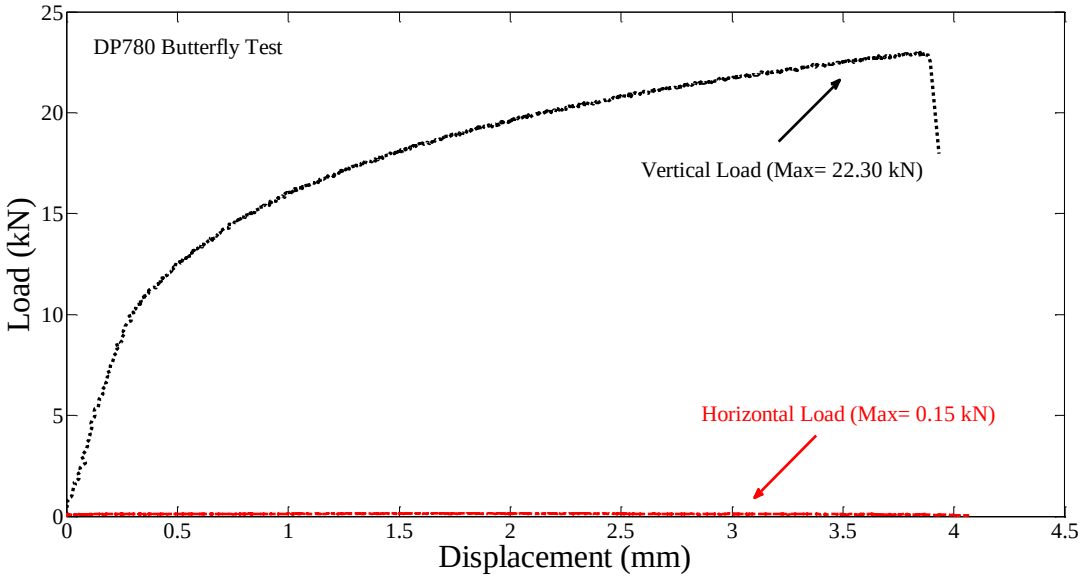

Fig.4. Comparison of vertical and horizontal loads for a DP780 butterfly test.

Similar to the mini-shear specimen, the butterfly samples were fabricated to have the applied load in the transverse direction for DP780 and the three orientations of 45°, 90° and 135°, for ZEK100. A 3.2 mm diameter with a corner radius end mill (0.02 rad corners) was used to reduce the thickness in the gauge section (*t* in Figure 2) to 0.95 mm for ZEK100 and 0.56 mm for DP780. A custom fixture was used to support the butterfly specimen to prevent buckling during machining. The butterfly specimens were carefully manually sanded using 320 and 500 grit silicon carbide sandpaper for DP780 and 800 and 1200 grit silicon carbide sandpaper for ZEK100 to remove machining marks in the gauge region (Figure 5). The tests were conducted with a cross-head velocity of 0.05 mm/s that leads to a von Mises equivalent strain rate of approximately 0.01 s^{-1} at the center of the specimen.

Fig.5. Butterfly specimen of ZEK100, before and after sanding.

Contrary to the mini-shear specimen that can be used to obtain stress-strain data under shear loading, any shear stress reported using the butterfly samples should be considered as a nominal shear stress and not be used in the development of a constitutive model due to the large gauge width of the butterfly specimen and non-uniform strain and stress distributions [29]. While a detriment in shear testing, the large gauge width of the butterfly is required since the sample can also be used to characterize fracture under other stress states [17], with triaxiality levels up to that of plane strain conditions (~0.58).

3.2. Elevated Strain Rates

Unfortunately, larger specimens with complex geometries and through-thickness machining, including the butterfly specimen, are not readily applicable for testing at higher rates. As shown by Walters [43], the edges of this type of specimen in the through-thickness machined sections

serve to diffract the stress waves passing through the material, making it difficult to achieve equilibrium within the specimen. Therefore, only the mini-shear specimen is used in the present work to study the shear response at higher rates of strain for ZEK100 sheet. However, the width of the mini-shear specimen developed by Piers *et al.* [27] is larger than the grip slot sizes of the testing apparatus available at University of Waterloo. Thus, the mini-shear specimen was modified for high-rate applications by scaling down all the dimensions of the specimen by 36% (Figure 6). It was shown by Rahmaan *et al*. [30] that the results of the reduced size mini-shear specimen are in excellent agreement with that of a full-size mini-shear sample for both an aluminium-magnesium alloy, AA5182-O, and a dual-phase steel, DP600. Therefore, in the present study, efforts to further validate the full-size versus scaled-down mini-shear specimens were not deemed necessary. The scaled-down mini-shear samples were fabricated by CNC machining using a 0.5 mm diameter flat end mill.

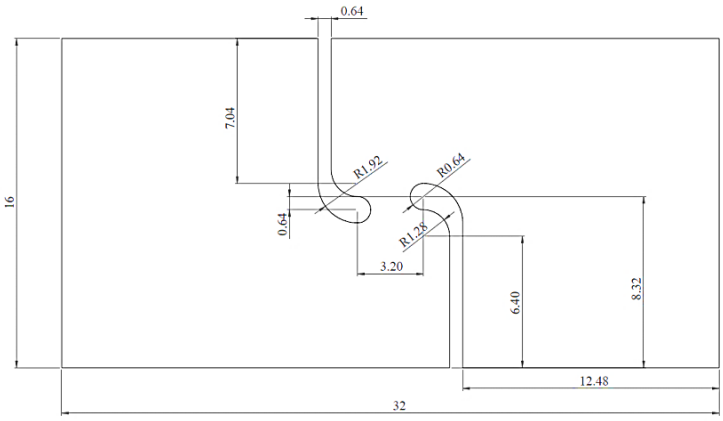

Fig.6. Scaled-down mini-shear specimen from Rahmaan *et al*. [30]. All dimensions are in millimeters.

The shear tests with elevated strain rates were performed using a Hydraulic Intermediate Strain Rate (HISR) testing machine [44] as shown in Figure 7. Cross-head velocities of 150 mm/s, and 900 mm/s were used to obtain von Mises equivalent true strain rates of 10 s^{-1} and 100 s^{-1}, respectively. To assess the repeatability of the experimental results, for all the shear tests, at least four specimens per orientation were tested. The evolution of the equivalent strain rates with deformation are presented in Figure 8 for the tests on ZEK100 along the 45° direction. It was

observed that the evolution of the strain rates in other directions are similar to that of the 45° direction and the results for the other directions are not shown here for brevity.

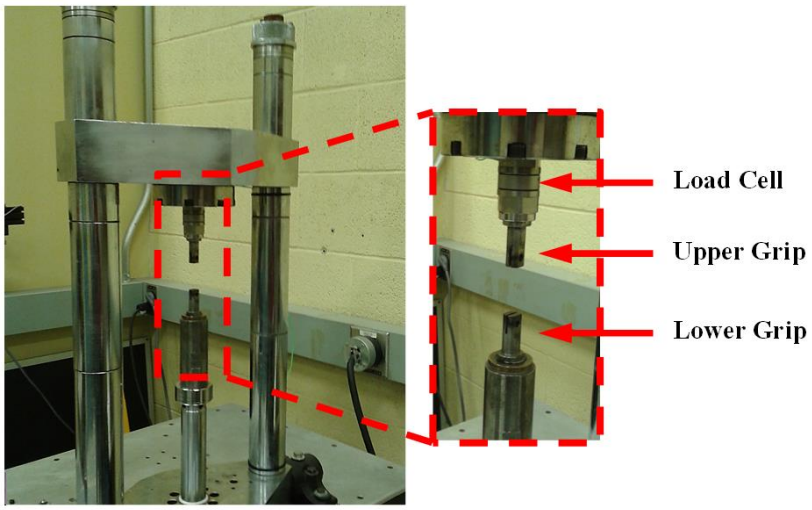

Fig.7. Schematic of the HISR machine.

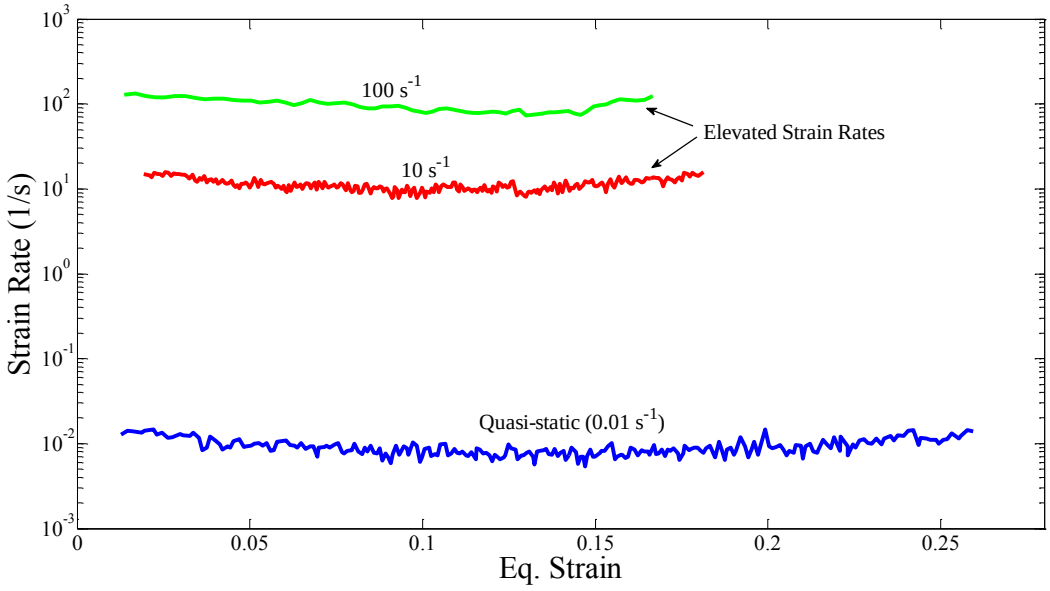

Fig.8. Evolution of the von Mises equivalent true strain rate with the von Mises equivalent strain for ZEK100 mini-shear specimen in 45° direction. Note that the quasi-static tests were performed with the full size mini-shear specimen and the tests at higher rates were done with the scaled-down mini-shear specimen.

3.3. Strain Measurements

The experiments were recorded using digital cameras to obtain full-field logarithmic strain measurements using digital image correlation (DIC) techniques, as described by Sutton *et al*. [45]. The commercial VIC2D and VIC3D DIC software packages from Correlated Solutions Inc. were used to obtain the full-field strain measurements. The resolutions in the DIC area of interest were 0.012 mm/pixel and 0.034 mm/pixel for the mini-shear and butterfly tests, respectively, and it was 0.016 mm/pixel for the scaled-down mini-shear tests. Stereo DIC was used for the butterfly shear tests with Point Grey 4.1 MP cameras with Xenoplan 35 mm (1:1.9) lenses at a rate of 5 frames per second with a DIC subset size of 25 pixels, a step size of 5 and a strain filter of 9 pixels. For the mini-shear specimens loaded at low quasi-static rates, a Point Grey 4.1 MP camera with a 60 mm (1:2.8) Nikon lens was used to acquire images at a rate of 5 frames per second. The DIC settings used a subset size of 29 pixels, step size of 5 and strain filter of 9 pixels.

For the elevated strain rate experiments, a high-speed Photron SA5 camera with a 105 mm (1:2.8) Sigma lens was used with frame rates of 18,600 and 40,000 frames per second for strain rates of 10 s^{-1} and 100 s^{-1}, respectively. A subset size of 25 pixels, step size of 4 and strain filter of 9 pixels were used for the tests with elevated strain rates.

Approximately 30 minutes before performing the tests, the samples were cleaned with acetone and then a white layer of Rust-Oleum® Painter's Touch primer was sprayed on the surface of the specimens. Then the black speckles were applied using Rust-Oleum® Painter's Touch spray paint to provide a speckle pattern for DIC measurements.

All strains reported in the present paper are based on the logarithmic (Hencky) definition of strain. The reported DIC strains were averaged using a circle with 0.5 mm diameter located at the center of the butterfly and full-size mini-shear specimens, while a circle diameter of 0.25 mm was used for the scaled-down mini-shear specimen. More information regarding the method of extracting the average local strains in the mini-shear specimen can be found in Rahmaan *et al*. [30].

All strain measurements for the mini-shear tests were obtained using 2-D digital image correlation techniques. Abedini *et al*. [29] compared both stereo and 2-D DIC of the mini-shear

specimen and reported that the simpler 2-D DIC system was sufficient to characterize both the shear stress and fracture response. However, to verify this further, two mini-shear tests were performed on ZEK100 in 135° orientation using 2-D and stereo DIC techniques with the same setup (Point Grey 4.1 MP camera with a 60 mm Nikon lens at a rate of 5 frames per second with a subset size of 29 pixels, step size of 5 and strain filter of 9 pixels). Figure 9 shows the evolution of shear strain with respect to displacement, confirming that the two techniques resulted in almost identical results for tests with the mini-shear specimen.

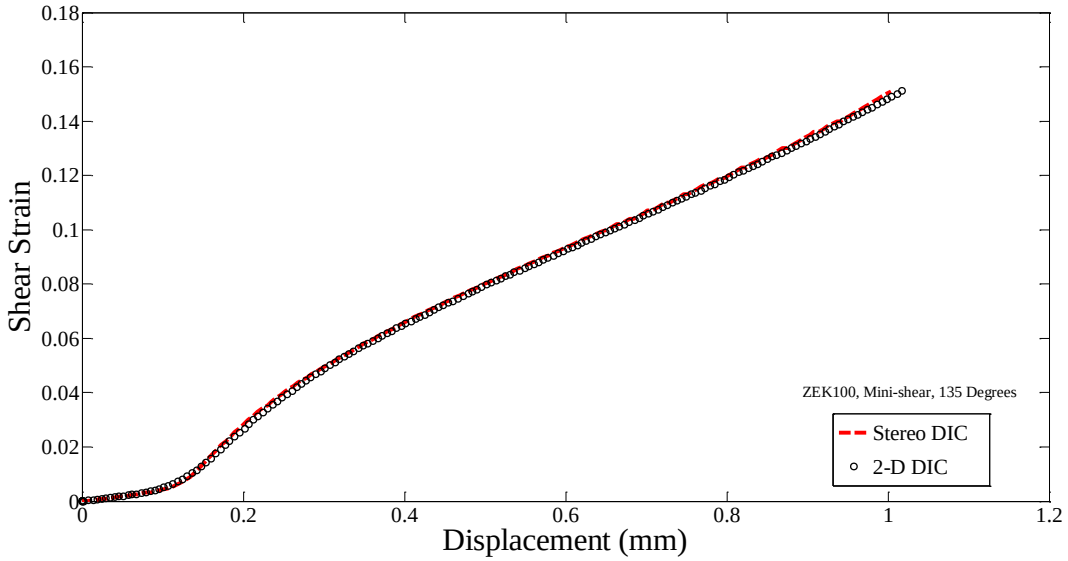

Fig.9. Comparison between 2-D and stereo DIC techniques for ZEK100 mini-shear test in 135° orientation with respect to the rolling direction.

As described earlier, the equivalent strain and the equivalent strain rate in the DIC software were computed using the common von Mises definition. While sufficient for DP780 steel, ZEK100 magnesium does not obey the von Mises yield criterion which is the case for other magnesium alloys such as AZ31B [46]. However, an anisotropic equivalent strain measure requires knowledge of the appropriate yield function and its coefficients which are not known in advance before constitutive characterizations. The von Mises equivalent measures are convenient, albeit simplistic, approximations for ZEK100 with the advantage that no anisotropy coefficients or material parameters are required.

4. Results and Discussion

4.1. Validation of the Shear Loading Condition

Figure 10 shows the measured DIC contours of shear strain in the mini-shear and butterfly specimens. As is apparent from Figure 10, the shear strain is concentrated in the gauge area of both specimens. The assumption of a simple shear loading condition until fracture can be evaluated by comparing the measured principal strains from the DIC analysis with the theoretical pure shear strain path, $\varepsilon_1 = -\varepsilon_2$. This validation is independent of the yield criterion since it does not involve the equivalent strain measure. A comparison of the measured strain paths for DP780 butterfly and mini-shear specimens are presented in Figure 11. Both geometries promote strain histories in excellent agreement with the theoretical pure shear condition for small strains while they marginally deviate from the ideal shear condition with larger deformation. Thus, the loading condition is reasonably close to the shear state even for the large strain levels attainable in shear testing of DP780.

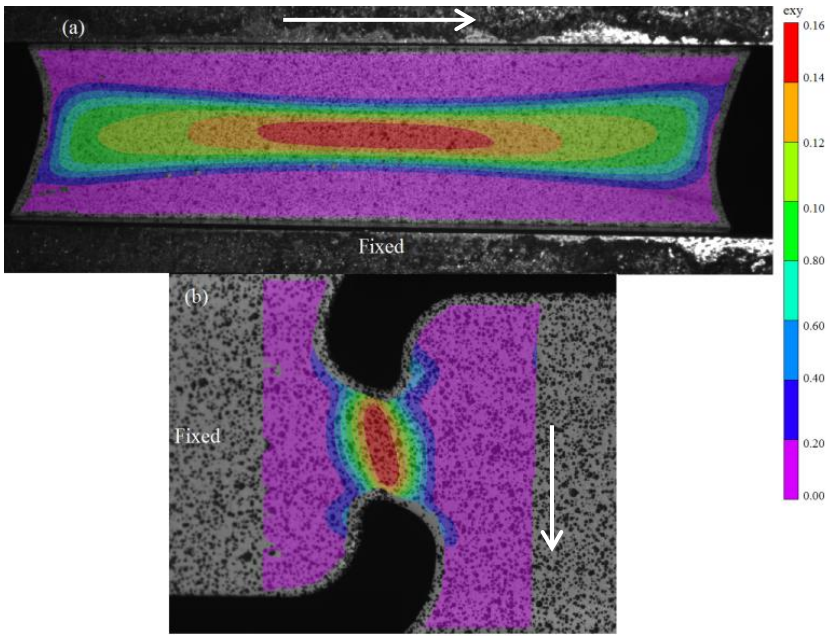

Fig.10. Contours of the shear strain for ZEK100 obtained with the DIC method for the (a) butterfly and (b) mini-shear specimens.

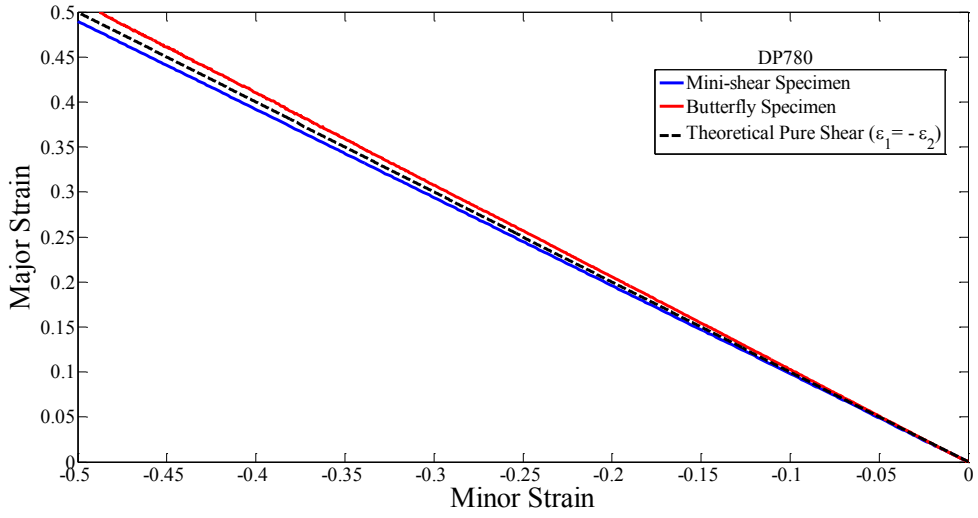

Fig.11. Comparison of the principal strains with the theoretical pure shear state.

For the isotropic DP780, it is possible to relate the strain increments ratio, α, to the stress ratio, β, using the Levy-Mises relation [47]:

$$\beta = \frac{2\alpha + 1}{2 + \alpha} \tag{2}$$

where

$$\alpha = \frac{d\varepsilon_2}{d\varepsilon_1} \text{ and } \beta = \frac{\sigma_2}{\sigma_1} \tag{3,4}$$

in which σ_1 and σ_2 are the major and minor stresses, and $d\varepsilon_1$ and $d\varepsilon_2$ are the major and minor strain increments, respectively. Then assuming the von Mises yield criterion for DP780, the stress triaxiality (ratio of the mean stress over the equivalent stress), η, can be obtained by:

$$\eta = \frac{\beta + 1}{3\sqrt{\beta^2 - \beta + 1}} \tag{5}$$

Using Eq. (5), the triaxiality evolution of DP780 was calculated by means of the strains measured from the DIC method, and the results are plotted in Figure 12 versus major strain for

the mini-shear and butterfly specimens. It can be seen from Figure 12 that although there are some levels of DIC noise for strain increments ratios, for both DP780 specimens the triaxiality remains close to the desired zero value (shear state) up to large strain values. Note that Eq. (5) is not applicable for the anisotropic ZEK100 sheet due to the assumption of isotropy through the von Mises criterion to derive Eq. (5).

It is important to mention that there will be some amount of rotation of the shear bands in these shear tests that might influence the behaviour of anisotropic materials. The rotation increases with deformation; therefore, it is more pronounced for higher strains and materials with high ductility. It is shown in Abedini *et al*. [29] that the shear band rotation is about 5.5° for ZEK100 due to its low ductility, while it is about 18° for DP780. Fortunately, DP780 response does not appear to be particularly sensitive to the loading direction so this rotation is not expected to be a significant issue for DP780, while the rotation in ZEK100 specimens is small.

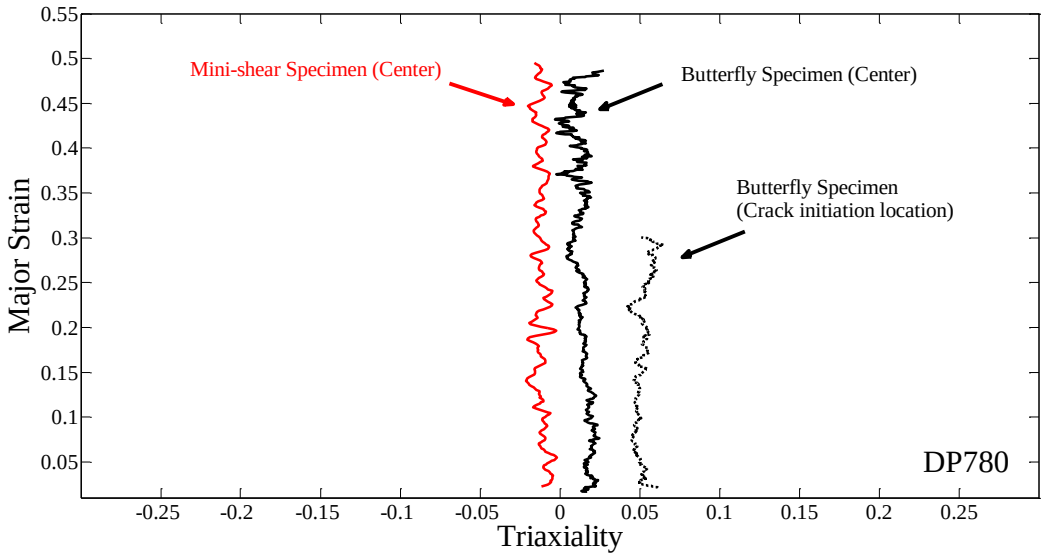

Fig.12. Evolution of the stress triaxiality for the mini-shear and butterfly tests of DP780.

4.2. Failure Characterization

For each geometry, the equivalent strains were obtained at the center of the gauge area in the last DIC image before the crack was visible. The fracture strains are local strains that were calculated using the DIC method for the mini-shear and butterfly specimens as explained in Section 3.3. For the mini-shear sample, the crack initiation site could not be identified for DP780 or ZEK100 which exhibited abrupt fracture. As a result, the equivalent strains were reported in the center of the mini-shear sample where the strains where highest. It was shown by Peirs *et al*. [27] and Abedini *et al*. [29] that fracture initiated in the center of mini-shear samples for Ti6Al4V, and DP600 alloys, respectively.

The fracture location for the butterfly specimen was discernable for both of the materials. Fracture occurred in the center of the gauge region for ZEK100 while for DP780, cracking initiated away from the center and close to the edge of the reduced thickness region where strains were lower than at the center. Furthermore, the triaxiality of the crack initiation point is shown in Figure 12 where the triaxiality is slightly higher than the central region suggesting a combined shear and tension mode at the crack initiation location. It should be emphasized that the DIC method provides full-field strain measurements on the surface of specimens; therefore, the triaxiality values reported in Figure 12 are from the specimen surface. It was shown in Dunand and Mohr [17] that the off-centre crack can probably be initiated below the visible surface where the stress triaxiality is higher than that of specimen's surface. To provide a lower bound estimate for the shear fracture strain, the strains were extracted from the center of the shear zone and not from the crack location.

The variation in the fracture location between ZEK100 and DP780 is likely a consequence of the butterfly geometry and the relative ductility of the alloys. An inspection of the shear band prior to fracture using the maximum shear strain rate in Figure 13 highlights the fracture locations in ZEK100 and DP780. The shear band in ZEK100 butterfly sample is concentrated in the center of the specimen and has not undergone a significant rotation due to its failure at relatively small strains. For DP780, which has a larger fracture strain than ZEK100, the shear band has undergone a larger shear-induced rotation and has the potential to interact with shoulder of the sample where the thickness is reduced, thereby increasing the likelihood of initiating fracture at a local discontinuity near the shoulder such as a machining defect, for example.

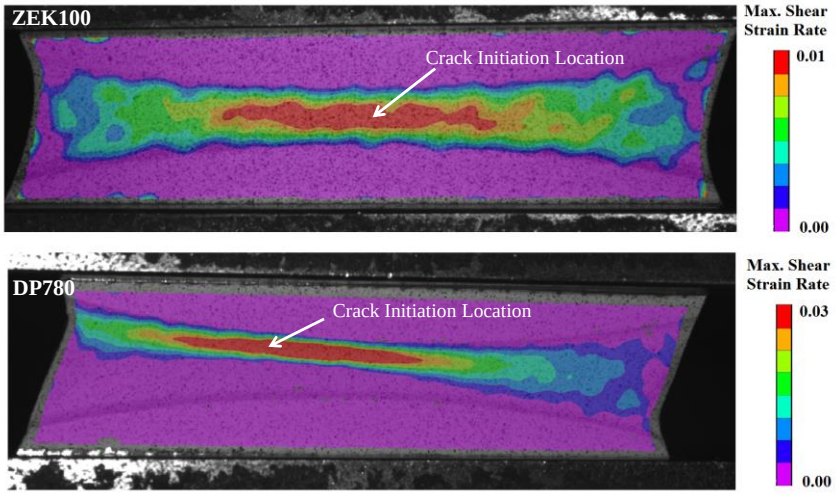

Fig.13. Contours of the maximum shear strain rate prior to fracture for ZEK100 and DP780 butterfly samples.

The contours of the maximum shear strain rate in ZEK100 and DP780 mini-shear samples are shown in Figure 14. Similar to the butterfly test, the shear band has undergone a larger rotation in DP780 compared to ZEK100. Due to the small gauge section of the mini-shear specimen, the shear strain rate is relatively uniform and highly localized with a strain rate near zero outside the gauge section.

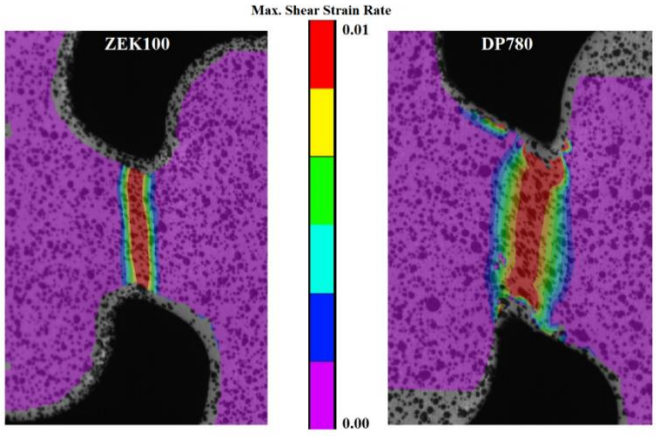

Fig.14. Contours of the maximum shear strain rate in the mini-shear samples prior to fracture for ZEK100 and DP780.

Tables 3 and 4 present the fracture strains for ZEK100 and DP780, respectively. In order to better show the anisotropic response of ZEK100, the fracture strains are also plotted in Figure 15 with respect to the testing orientation. It can be seen from Figure 15 that the equivalent fracture strains of ZEK100 are highest for 90° and lowest for 135° orientations. Overall, the strains at fracture for ZEK100 are relatively low compared to a value of over 60% for DP780. Comparing the two shear geometries, the butterfly specimens always displayed the largest variation in the fracture strains. Furthermore, the butterfly specimens resulted in lower fracture strains compared with the mini-shear specimens as demonstrated in Tables 3 and 4 and Figure 15. As mentioned earlier, at least four tests were conducted for each material and orientation. However, for the case of the butterfly specimens for DP780, six additional tests were performed since there was a large variation in fracture strain and fracture location. The generally lower failure strains with higher variability in the butterfly samples could be the result of machining-induced defects during the through-thickness machining of the butterfly gauge region. Therefore, shear specimens without through-thickness machining are preferred for fracture characterization under shear loading conditions to reduce uncertainties and imperfections from the machining process. Furthermore, for materials with variation of properties through the sheet thickness, specimens with through-thickness machined regions characterize the sheet properties near the mid-plane, while specimens without through-thickness machining provide a more representative average response of the sheet in shear loading condition.

Table.3. Fracture strains of DP780.

Butterfly		**Mini-shear**	
Fracture Strain	**Standard Deviation**	**Fracture Strain**	**Standard Deviation**
0.614	0.129	0.661	0.014

Table.4. Fracture strains of ZEK100.

	Quasi-static (Butterfly)		Quasi-static (Mini-shear)		10 s^{-1} (Mini-shear)		100 s^{-1} (Mini-shear)	
Orientation	Fracture Strain	Standard Deviation	Fracture Strain	Standard Deviation	Fracture Strain	Standard Deviation	Fracture Strain	Standard Deviation
45°	0.198	0.005	0.263	0.005	0.195	0.003	0.196	0.003
90°	0.263	0.014	0.285	0.007	0.205	0.004	0.206	0.008
135°	0.192	0.013	0.217	0.004	0.194	0.004	0.196	0.004

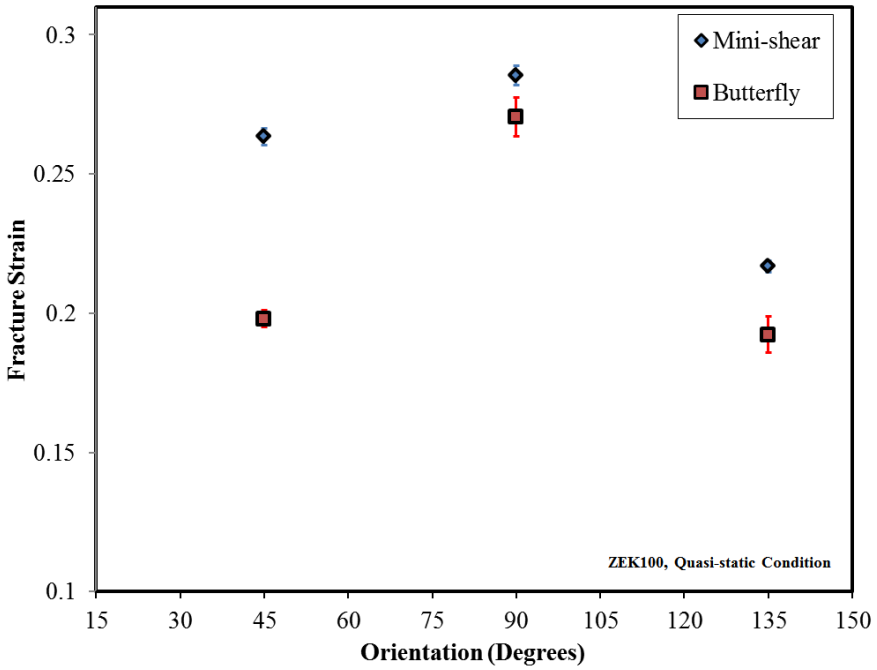

Fig.15. Fracture strains with respect to the sheet orientation for ZEK100 at quasi-static condition.

As mentioned earlier, the strains reported in the present paper are the average values over a circle in the gauge area of the specimens. Rahmaan *et al*. [30] studied the influence of the method of averaging the DIC shear strain by using points, squares, and circles with different sizes in the mini-shear specimen. However, in order to investigate the influence of the method of averaging strains, two different circle sizes, one smaller (R_1=0.25mm), and one larger (R_3=0.75mm) than the reference circle size of R_2=0.5mm along with a point at the center of circles (Figure 16) were used to obtain the fracture strains of DP780 mini-shear and butterfly experiments and the results are presented in Table 5. It can be seen that as the size of the circles

gets smaller, larger fracture strains are reported; however, the same trend in ranking of the mini-shear versus butterfly specimens for the reported failure strains is observed.

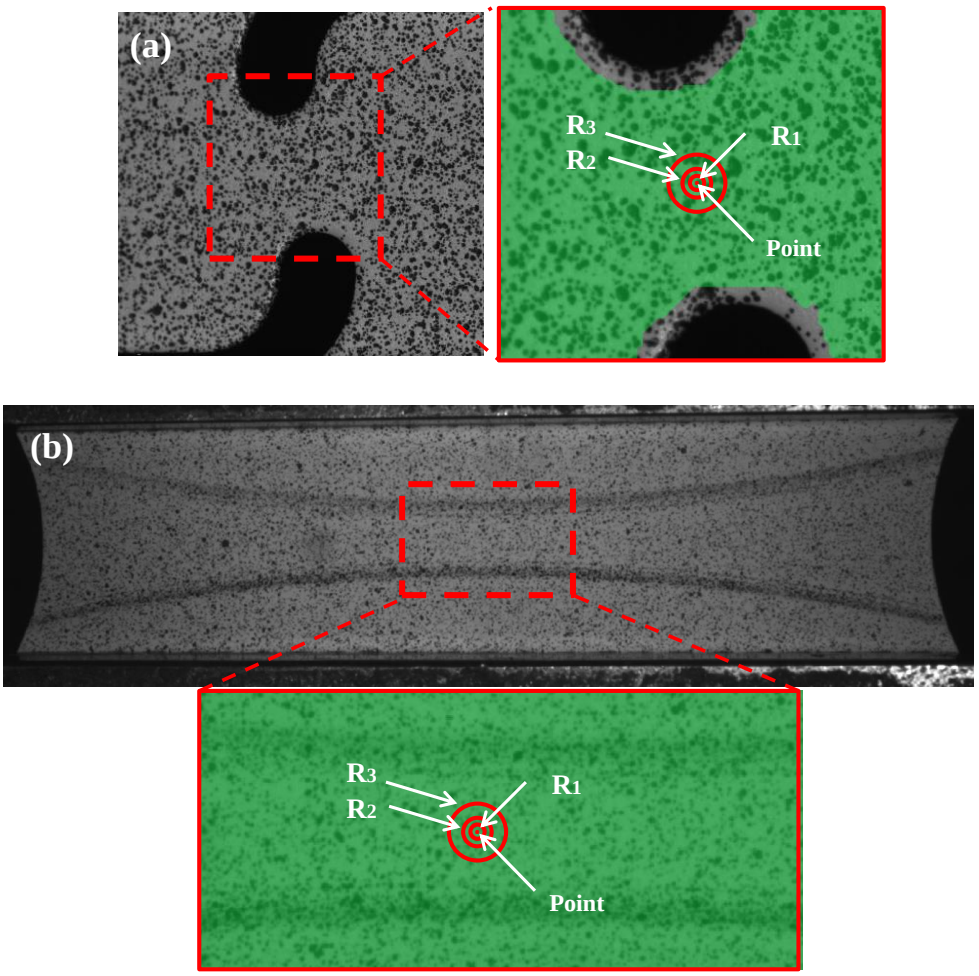

Fig.16. Three circle sizes with different radii (R_1=0.25mm, R_2=0.5mm, R_3=0.75mm) and a point at the center of the circles were used to evaluate the influence of the size of the area where the strain are averaged.

Table.5. Influence of the circle size on measured fracture strains for DP780.

Specimen	Min-shear				Butterfly			
Circle radius (mm)	0 (point)	0.25	0.5	0.75	0 (point)	0.25	0.5	0.75
Fracture Strain	0.695	0.686	0.661	0.643	0.641	0.628	0.614	0.597
Standard Deviation	0.018	0.015	0.014	0.014	0.136	0.130	0.129	0.126

The effect of strain rate on fracture strains for ZEK100 is examined in Figure 17 (the measured data is also reported in Table 4). It should be mentioned that a similar number of images were captured by the DIC method for the strain rates of 0.01 and 10 s^{-1} (approximately 360 images), while a lower number of images (120 or one-third of that of other rates) were recorded for the strain rate of 100 s^{-1} due to the maximum frame rate (at the same spatial resolution) of the high speed cameras. It is observed from Figure 17 that the fracture strains decrease with increasing strain rate from quasi-static to elevated strain rates while there are not significant differences between the results at strain rates of 10 s^{-1} and 100 s^{-1}. In addition, although the same trend for anisotropic response is preserved for fracture strains under elevated strain rates, the difference in the measured fracture strains for different loading directions is reduced at elevated rates of strain. However, this behaviour may be associated with a shift in failure mechanism associated with adiabatic heating effects as strain rate increases [48-49].

To compare the distribution of the shear strains at different strain rates, a “line inspector tool” or “line slice” was defined in the gauge area (Figure 18) to plot the DIC shear strains across the path defined by the line slice for both the quasi-static and 100 s^{-1} tests. Figure 18 shows the normalized strains by the maximum strain of the path (occurring at the center of the gauge section) versus the normalized distance over the path for the two strain rates. The strain values in Figure 18 are from the last image prior to fracture for the tests in the 90° direction. It is apparent that the strains are highest at the center of the gauge section while it can be seen that for the elevated rate, the slope of the curve is higher than its quasi-static counterpart, suggesting that strains tend to localize more severely at higher rates which may lead to localized adiabatic shear bands. Further study of this behaviour of for ZEK100 sheet will be addressed in future work.

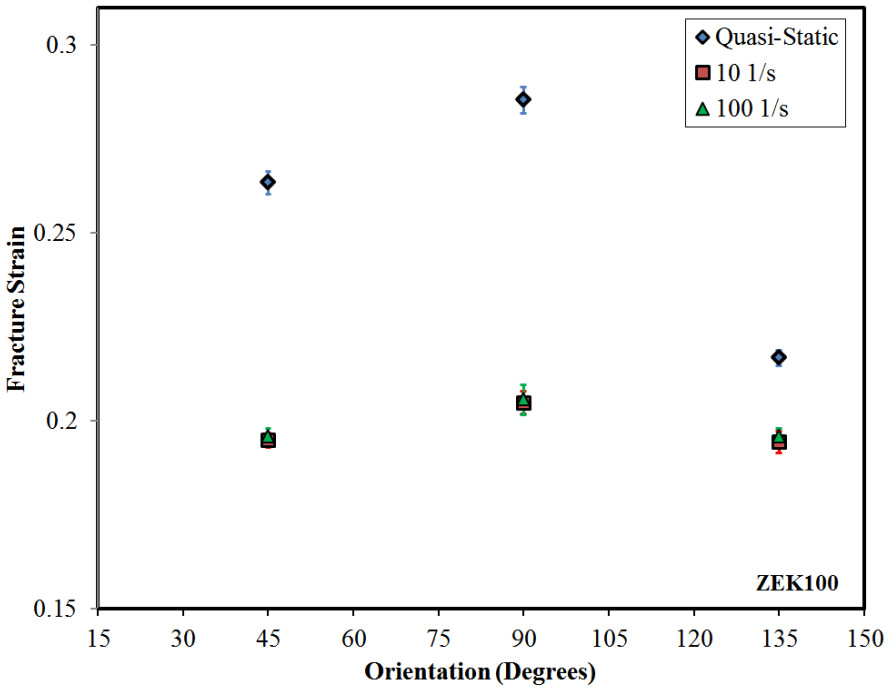

Fig.17. Fracture strains with respect to the sheet orientation and strain rate for ZEK100 obtained with the mini-shear specimen.

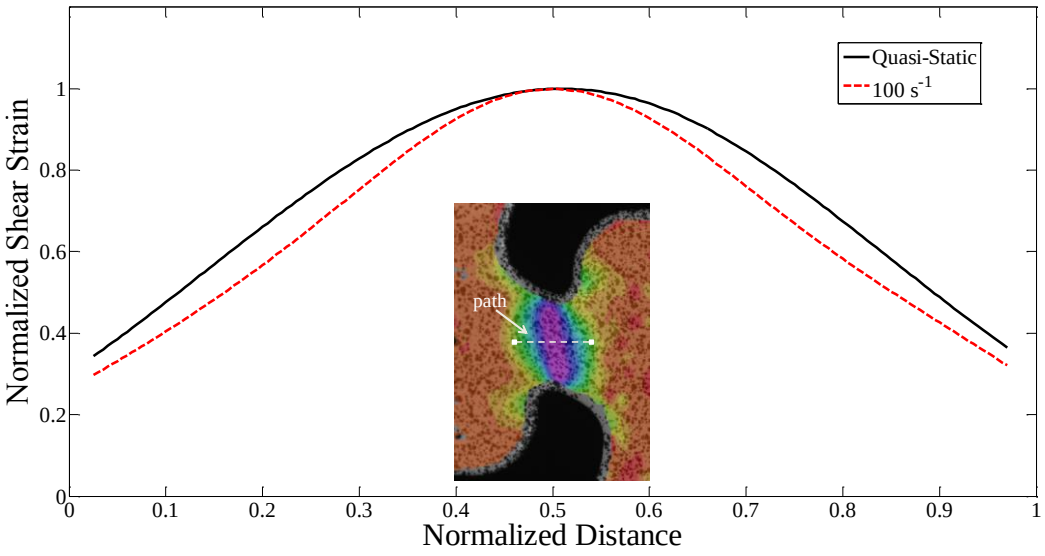

Fig.18. Normalized shear strain with respect to the normalized distance over the path for the ZEK100 mini-shear samples tested in 90° orientation. The shear strain was normalized by the maximum shear strain in the path for each geometry.

5. Conclusions

The fracture behaviour of two automotive alloys (ZEK100 and DP780) was examined in shear loading conditions using two different test geometries (mini-shear and butterfly specimens) adopted from the literature. The response of ZEK100 alloy showed significant anisotropy of the fracture strains. In addition, the butterfly specimen resulted in lower fracture strains and inconsistency in fracture location which could be caused by the through-thickness machining of a large region of the sample. Shear tests at elevated strain rates were performed on ZEK100 with the scaled mini-shear specimen where fracture strains decreased with increased strain rate. It was also observed that the fracture strains exhibit a reduced orientation dependency at higher strain rates.

Overall, the butterfly test specimen is a useful test geometry that can be used for quasi-static fracture characterization in stress states ranging from shear to plane strain. For shear loading, the butterfly shear fracture strains have similar trends to that of the mini-shear geometry albeit with lower failure strains and larger variations. Although it lacks the versatility of the butterfly geometry, the mini-shear specimen has the advantage of being easier to fabricate and is readily amenable to high rate and elevated temperature testing since it can be used on conventional tensile testing machines or in high rate experiments. Additionally, the mini-shear sample can be used for constitutive characterization.

Acknowledgements

Financial support for this work provided by Cosma International, Automotive Partnership Canada, the Ontario Research Fund, the Natural Sciences and Engineering Research Council of Canada, the Canada Research Chairs Secretariat, and the Canada Foundation for Innovation is thankfully acknowledged. The authors would like to thank Mark Kuntz at the University of Waterloo engineering machine shop for fabricating the specimens.

References

[1] Bai Y, Wierzbicki T (2008) A new model of metal plasticity and fracture with pressure and Lode dependence. Int J Plasticity 24:1071-1096.

[2] Bai Y, Wierzbicki T (2010) Application of extended Mohr-Coulomb criterion to ductile fracture. Int J Fracture 161:1-20.

[3] Roth C C, Mohr D (2015) Ductile fracture experiments with locally proportional loading histories. Int J Plasticity doi: 10.1016/j.ijplas.2015.08.004.

[4] Montheillet F, Cohen M, Jonas J J (1984) Axial stresses and texture development during the torsion testing of Al, Cu and α-Fe. Acta Metall 32(11):2077-2089.

[5] Yoshida K, Ishii A, Tadano Y (2014) Work hardening behavior of polycrystalline aluminum alloy under multiaxial stress paths. Int J Plasticity 53:17-39.

[6] Stout M G, O'Rourke J A (1989) Experimental deformation textures of OFE copper and 70:30 brass from wire drawing, compression, and torsion. Metal Trans A 20A:125-131.

[7] Peirs J, Verleysen P, Tirry W, Rabet L, Schryvers D, Degrieck J (2011) Dynamic shear localization in Ti6Al4V. Eng Procedia 10:2342-2347.

[8] Gray III G Y, Vecchio K S, Livescu V (2016) Compact forced simple-shear for studying localization in materials. Acta Mater 103:12-22.

[9] Iosipescu N (1967) New accurate procedure for single shear testing of metals. Journal of Materials 2:537-566.

[10] Gasperini M, Pinna C, Swiatnicki W (1996) Microstructure evolution and strain localization during shear deformation of an aluminum alloy. Acta Mater 44(10):4195-4208.

[11] Bae D G, Ghosh A K (2003) A planar simple shear test and flow behavior in a superplastic Al-Mg alloy. Metall Mater Trans 34:2003-2465.

[12] Bouvier S, Haddadi H, Levee P, Teodosiu C (2006) Simple shear tests: Experimental techniques and characterization of the plastic anisotropy of rolled sheets at large strains. Mater Technol 172:196-103.

[13] Rauch E F (2009) Plastic behavior of metals at large strains: experimental studies involving simple shear. Eng Mater Technol 131(1) 0111107-1-8.

[14] Carbonniere J, Thuillier S, Sabourin F, Brunet M, Manach P Y (2009) Comparison of the work hardening of metallic sheets in bending-unbending and simple shear. Int J Mec Sci 51:122-130.

[15] Thuillier S, Manach P Y (2009) Comparison of the work-hardening of metallic sheets using tensile and shear strain paths. Int J Plasticity 25:733-751.

[16] Mohr D, Henn S (2007) Calibration of stress-triaxiality dependant crack formation criteria: a new hybrid experimental-numerical method. Exp Mech 47:805-820.

[17] Dunand M, Mohr D (2011) Optimized butterfly specimen for the fracture testing of sheet materials under combined normal and shear loading. Eng Frac Mech 78:2919-2934.

[18] Bao Y B, Wierzbicki T (2004) On fracture locus in the equivalent strain and stress triaxiality space. Int J Mech Sci 46(1):81-98.

[19] Tarigopula V, Hopperstad O S, Langseth M, Clausen A H, Hild F, Lademo O G, Eriksson M (2008) A study of large plastic deformations in dual phase steel using digital image correlation and FE analysis. Exp Mech 48(2):181-196.

[20] Brunig M, Chyra O, Albrecht D, Driemeier L, Alves M (2008) A ductile damage criterion at various stress triaxialities. Int J Plasticity 24:1731-1755.

[21] Kang J, Wilkinson D S, Wu P D, Bruhis M, Jain M, Embury J D, Mishra R K (2008) Constitutive behaviour of AA5754 sheet materials at large strains. Eng Mater Technol 130:1-5.

[22] Lademo O G, Engler O, Keller S, Berstad T, Pedersen K O, Hopperstad O S (2009) Identification and validation of constitutive model and fracture criterion for AlMgSi alloy with application to sheet forming. Materials and Design 30:3005-3019.

[23] Reyes A, Eriksson M, Lademo O G, Hopperstad O S, Langseth M (2009) Assessment of yield and fracture criteria using shear and bending tests. Material and Design 30:596-608.

[24] Gao F, Gui L, Fan Z (2011) Experimental and numerical analysis of an in-plane shear specimen designed for ductile fracture studies. Exp Mech 51:891-901.

[25] Gruben G, Fagerholt E, Hopperstad O S, Borvik T (2011) Fracture characteristics of a cold-rolled dual-phase steel. European Journal of Mechanics A/Solids 30:204-218.

[26] Lian J, Sharaf M, Archie F, Munstermann S (2012) A hybrid approach for modelling of plasticity and failure behaviour of advanced high-strength steel sheets. Int J Damage Mech 22(2):188-21.

[27] Peirs J, Verleysen P, Degrieck J (2012) Novel technique for static and dynamic shear testing of Ti6Al4V sheet. Exp Mech 52:729-741.

[28] Peirs J, Verleysen P, Van Paepegem W, Degrieck J (2011) Determining the stress-strain behaviour at large strains from high strain rate tensile and shear experiments. Int J Impact Eng 38:406-415.

[29] Abedini A, Butcher C, Anderson D, Worswick M J, Skszek T (2015) Fracture characterization of automotive alloys in shear loading. SAE International Journal of Materials and Manufacturing 8(3).

[30] Rahmaan T, Butcher C, Abedini A, Worswick M (2015) Effect of strain rate on shear properties and fracture characteristics of DP600 and AA5182-O sheet metal alloys. Proceedings of the 11th International DYMAT Conference.

[31] Campbell J D, Fergusen W G (1970) The temperature and strain-rate dependence of the shear strength of mild steel. Philosophical Magazine 21:169, 63-82.

[32] Klepaczko J R (1994) An experimental-technique for shear testing at high and very high strain rates-the case of a very mild steel. Int J Impact Eng 15:25-39.

[33] Klepaczko J R, Nguyen H V, Nowacki W K (1999) Quasi-static and dynamic shearing of sheet metals. European Journal of Mechanics A/Solids 18:271-289.

[34] Rusinek A, Klepaczko J R, (2001) Shear testing of a sheet steel at wide range of strain rates and a constitutive relation with strain-rate and temperature dependence of the flow stress. Int J Plasticity 17:87-115.

[35] Bonnet-Lebouvier A S, Klepaczko J R (2002) Numerical study of shear deformation in Ti-6Al-4V at medium and high strain rates, critical impact velocity in shear. Int J Impact Eng 27(7):755-769.

[36] Hubnatter W, Merklein M (2008) Characterization of material behavior under pure shear condition. Int J Mater Form 1:233-236.

[37] Guo Y, Li Y (2012) A novel approach to testing the dynamic shear response of Ti-6Al-4V. Acta Mechanica Solida Sinica 25(3):299-311.

[38] Shi F F, Merle R, Hou B, Liu J G, Li Y L, Zhao H (2014) A critical analysis of plane shear tests under quasi-static and impact loading. Int J Imp Eng 74:107-119.

[39] Till E, Hackl B (2013) Calibration of plasticity and failure models for AHSS sheets. Proceedings of the International Deep Drawing Research Conference (IDDRG).

[40] Winkler S, Thomson A, Salisbury C, Worswick M, Van Riemsdijk I, Mayer R (2008) Strain rate and temperature effects on the formability and damage of advanced high strength steels. Metall Mater Trans A 39(6):1350-1358.

[41] Kurukuri S, Worswick M J, Bardelcik A, Mishra R K, Carter J T (2014) Constitutive behavior of commercial grade ZEK100 magnesium alloy sheet over a wide range of strain rates. Metall Mater Trans A 45:3321-3337.

[42] Lopes A B, Barlat F, Gracio J J, Ferreira Duarte J F, Rauch E F (2003) Effect of texture and microstructure on strain hardening anisotropy for aluminum deformed in uniaxial tension and simple shear. Int J Plasticity 19:1-22.

[43] Walters C L (2009) Development of a punching technique for ductile fracture testing over a wide range of stress states and strain rates. PhD Dissertation, Massachusetts Institute of Technology.

[44] Bardelcik A, Worswick M J, Wells M A (2014) The influence of martensite, bainite and ferrite on the as-quenched constitutive response of simultaneously quenched and deformed boron steel – Experiments and model. Materials and Design 55:509-525.

[45] Sutton M A, Orteu J, Schreier H W (2009) Image correlation for shape, motion and deformation measurements. Springer.

[46] Ghaffari Tari D, Worswick M J, Ali U, Gharghouri M A (2014) Mechanical response of AZ31B magnesium alloy: Experimental characterization and material modeling considering proportional loading at room temperature. Int J Plasticity 55:247-267.

[47] Jia Y, Bai Y (2016) Experimental study on the mechanical properties of AZ31B-H24 magnesium alloy sheets under various loading conditions. Int J Fract 197:25-48.

[48] Mason C, Worswick M, Gallagher P (2007) Adiabatic shear in Remco iron and quenched and tempered 4340 steel. Journal de Physique **7**:827-832.

[49] Mason C, Worswick M J (2001) Adiabatic shear in annealed and shock-hardened iron and in quenched and tempered 4340 steel. Int. J. Fract 111:29-51.